Electronic Supplementary Information

$PbTeB_4O_9$: A Lead Tellurium Borate with Unprecedented Fundamental Building Block [B_4O_{10}] and Large Birefringence

Ruonan Zhang,[a,b] Abudukadi Tudi,[a,b] Xia Yang,[a,b] Xuping Wang,[a] Zhihua Yang,[a] Shujuan Han*[a] and Shilie Pan*[a]

[a]Research Center for Crystal Materials; State Key Laboratory of Functional Materials and Devices for Special Environmental Conditions; Xinjiang Key Laboratory of Functional Crystal Materials; Xinjiang Technical Institute of Physics & Chemistry, CAS, 40-1 South Beijing Road, Urumqi 830011, China. E-mails: hansj@ms.xjb.ac.cn, slpan@ms.xjb.ac.cn.

[b]Center of Materials Science and Optoelectronics Engineering, University of Chinese Academy of Sciences, Beijing 100049, China

Experimental Section

Synthesis. Crystals of $PbTeB_4O_9$ were synthesized *via* high temperature solution method in open air. A mixture of TeO_2 (0.261 g, 0.0016 mol), $PbCO_3$ (0.434 g, 0.0016 mol) and H_3BO_3 (0.304 g, 0.0049 mol) was mixed in an agate mortar, and then moved to a platinum crucible, which were placed in a homemade furnace. The samples were heated to 500 °C in 10 h, held for 12 h, then cooled to 400 °C at a rate of 1 °C/h, and then cooled to the room temperature at a rate of 15 °C/h. Small single crystals were found in the platinum crucible after growth and several single crystals were picked up for further single crystal X-ray diffraction measurements.

The polycrystalline sample of $PbTeB_4O_9$ was obtained by solid-state reaction method by mixing TeO_2, $PbCO_3$ and H_3BO_3 according to the stoichiometric ratio. The mixture was preheated at 300 °C for 12 h. After that, the temperature was gradually raised to 520 °C with several intermediate grinding and mixing, and then held at a certain temperature for 3 days. Powder X-ray diffraction (PXRD) data were collected to verify the purity of polycrystalline sample.

Single-Crystal X-ray Diffraction. The single-crystal XRD data were collected on a Bruker D8 Venture diffractometer assembled with monochromatic Mo-Kα (λ = 0.71073 Å) as the radiation source at room temperature and then integrated by using the SAINT program.[1] All the structures were solved by direct methods and refined through the full-matrix least-squares fitting on F_2 with the OLEX2 software.[2] These structures were verified utilizing the ADDSYM algorithm from PLATON.[3] The final refined atomic positions and isotropic thermal parameters, selected bond lengths, and angles for the title compounds are given in Tables S2–S3. The structural rationality of the title compound is also evident from bond valence sum (BVS) calculations (Table S2).[4]

Powder X-ray Diffraction. Powder XRD data were collected with a Bruker D2 PHASER diffractometer equipped with Cu Kα radiation (λ = 1.5418 Å) at room temperature. Data were collected in the angular (2θ) ranging from 10 to 70 ° with a scan step width and a fixed counting time of 0.02 ° and 1 s/step, respectively.

Thermal Analysis. Thermogravimetric analyses (TGA) and differential scanning calorimetry (DSC) were measured on a NETZSCH STA 449 F3 simultaneous analyzer instrument. The polycrystalline powders were placed in a Pt crucible and heated from room temperature to 800 °C at a rate of 5 °C·min^{-1} under a constant flow of nitrogen gas.

Energy Dispersive X-ray Spectroscope (EDS). EDS was measured on a SUPRA 55VP field emission scanning electron microscope equipped with a BRUKER X-ray Flash-SDD-5010 energy-dispersive X-ray spectroscope.

Infrared Spectroscopy. The infrared spectra were recorded using a Shimadzu IRAffinity-1 Fourier transform infrared spectrometer within the range of 400–4000 cm^{-1}. The sample was mixed with dried KBr.

UV−Vis−NIR Diffuse Reflectance Spectroscopy. The diffuse reflectance spectra were measured by using a Shimadzu Solid Spec-3700 DUV spectrophotometer in the wavelength range of 200–2600 nm at room temperature.

Computational Methods. The electronic and band structures of title compounds were calculated using a plane-wave pseudo-potential total energy package, CASTEP.[5] The theoretical basis of CASTEP is density functional theory,[6] and the generalized gradient approximation (GGA) with the Perdew-Burke-Emzerhof (PBE) exchange-correlation functional[7] was chosen for all calculations. Adopting the norm-conserving pseudopotential (NCP),[8,9] the following orbital electrons were treated as valence electrons: Pb: $6s^2$ $6p^2$, Te: $5s^2$ $5p^4$, B: $2s^2$ $2p^1$ and O: $2s^2$ $2p^4$. Besides, the kinetic energy cutoffs were chosen as 820.0 eV, and the numerical integration of the Brillouin zone was performed via using a 4×4×3 Monkhorst Pack[10] k-point sampling. The other calculation parameters and convergence criteria were the default values of the CASTEP code. The linear optical properties of $PbTeB_4O_9$ were examined based on the dielectric function $\varepsilon(\omega) = \varepsilon_1(\omega) + i\varepsilon_2(\omega)$. The imaginary part of dielectric function, $\varepsilon_2(\omega)$, can be calculated from the electronic transition between the occupied and the unoccupied states by the following formula:

$$\varepsilon_2(\omega) = \frac{4\pi^2}{\Omega}\lim_{q\to 0}\frac{1}{q^2}\times\sum_{c,v,k} 2\omega_k\delta(E_c - E_v - \omega)\,|\langle c|e\cdot q|v\rangle|^2$$

where Ω is the volume of the elementary cell, *v* and *c* depict the valence bands and the conduction bands, respectively, ω is the frequency of the incident light, the $\langle c | e \cdot q | v \rangle$ is the integrated optical transitions from the valance states to the conduction states. The real part, $\varepsilon_1(\omega)$, is obtained by the Kramers-Kronig transformation,[11] accordingly the refractive indices and the birefringence (Δn) can be calculated. Besides, the contribution of ionic groups was further investigated using the real space atom-cutting method.[12]

Table S1. Crystal data and structure refinement for $PbTeB_4O_9$.

Empirical formula	$PbTeB_4O_9$
Formula weight	522.03
Temperature	273.15 K
Wavelength	0.71073 Å
Crystal system, space group	Triclinic, $P\bar{1}$
Unit cell dimensions	a = 6.5740(3) Å α = 70.105(2)°
	b = 6.7445(3) Å β = 78.877(2)°
	c = 9.8903(5) Å γ = 61.726(2)°
Volume	362.89(3) Å^3
Z, Calculated density	2, 4.778 g/cm^3
Absorption coefficient	27.215 mm^{-1}
F(000)	452
θ range for data collection	2.191 to 27.507°
Limiting indices	$-8 \le h \le 8$, $-8 \le k \le 8$, $-12 \le l \le 12$
Reflections collected / unique	10162 / 1639 [R(int) = 0.0570]
Completeness	98.5 %
Maximum and minimum transmission	0.2632 and 0.1494
Refinement method	Full matrix least squares on F^2
Data / restraints / parameters	1639 / 0 / 137
Goodness-of-fit on F^2	1.112
Final R indices [$F_o^2 > 2\sigma(F_o^2)$][a]	R_1 = 0.0214, wR_2 = 0.0473
R indices (all data)[a]	R_1 = 0.0225, wR_2 = 0.0481
Extinction coefficient	0.0048(5)
Largest diff. peak and hole	1.292 and −1.220 e Å^{-3}

[a] $R_1 = \Sigma||F_o| - |F_c||/\Sigma|F_o|$ and $wR_2 = [\Sigma w(F_o^2 - F_c^2)^2/\Sigma wF_o^4]^{1/2}$ for $F_o^2 > 2\sigma(F_o^2)$

Table S2. Atomic coordinates (× 10^4) and equivalent isotropic displacement parameters ($A^2 \times 10^3$) and bond valence sum (BVS) calculation for $PbTeB_4O_9$. U_{eq} is defined as one third of the trace of the orthogonalized U_{ij} tensor.

atom	x	y	z	U_{eq} ($Å^2$)	BVS
Pb(1)	6542(1)	5744(1)	1368(1)	14(1)	1.76
Te(1)	3607(1)	3370(1)	4786(1)	14(1)	3.72
B(1)	1441(11)	6659(11)	2113(7)	14(1)	3.01
B(2)	3426(10)	2340(11)	2138(7)	12(1)	3.03
B(3)	7634(11)	-41(12)	1533(7)	13(1)	3.04
B(4)	815(11)	688(11)	1792(7)	12(1)	3.05
O(1)	2315(6)	8477(7)	1740(5)	14(1)	2.01
O(2)	1099(7)	5927(7)	3693(5)	15(1)	2.00
O(3)	3176(6)	4769(7)	1538(5)	12(1)	1.88
O(4)	3903(7)	1392(7)	3677(5)	17(1)	1.94
O(5)	1296(6)	2376(7)	1859(5)	14(1)	1.96
O(6)	-1545(6)	1416(7)	1708(5)	15(1)	2.17
O(7)	5348(6)	769(7)	1375(5)	15(1)	1.93
O(8)	9145(6)	-2257(7)	1510(5)	14(1)	1.99
O(9)	6014(7)	4148(8)	3842(5)	17(1)	1.74

Table S3. Selected bond lengths (Å) and angles (deg.) for $PbTeB_4O_9$.

Pb(1)-O(1)	2.544(4)	B(1)-O(1)	1.499(7)
Pb(1)-O(3)	2.553(4)	B(1)-O(2)	1.476(8)
Pb(1)-O(3)#1	2.971(4)	B(1)-O(3)	1.454(8)
Pb(1)-O(5)#2	2.876(4)	B(1)-O(8)#6	1.474(7)
Pb(1)-O(6)#2	2.497(4)	B(2)-O(3)	1.478(7)
Pb(1)-O(7)#3	3.098(4)	B(2)-O(4)	1.468(8)
Pb(1)-O(7)#1	2.937(4)	B(2)-O(5)	1.466(7)
Pb(1)-O(8)#3	2.678(4)	B(2)-O(7)	1.482(8)
Pb(1)-O(9)	2.346(4)	B(3)-O(6)#2	1.393(7)
Te(1)-O(2)	1.894(4)	B(3)-O(7)	1.355(7)
Te(1)-O(4)	1.919(4)	B(3)-O(8)	1.352(8)
Te(1)-O(4)#4	2.822(4)	B(4)-O(1)#7	1.356(7)
Te(1)-O(9)#5	2.604(4)	B(4)-O(5)	1.341(7)
Te(1)-O(9)	1.880(4)	B(4)-O(6)	1.399(7)
O(1)-Pb(1)-O(3)	55.17(12)	O(3)-B(1)-O(8)#6	113.5(5)
O(1)-Pb(1)-O(8)#3	108.81(12)	O(8)#6-B(1)-O(1)	109.2(5)
O(3)-Pb(1)-O(8)#3	163.46(12)	O(8)#6-B(1)-O(2)	106.5(5)
O(6)#2-Pb(1)-O(1)	129.69(12)	O(3)-B(2)-O(7)	110.3(5)
O(6)#2-Pb(1)-O(3)	76.23(12)	O(4)-B(2)-O(3)	112.0(5)
O(6)#2-Pb(1)-O(8)#3	118.00(12)	O(4)-B(2)-O(7)	108.1(5)
O(9)-Pb(1)-O(1)	79.78(14)	O(5)-B(2)-O(3)	107.3(4)
O(9)-Pb(1)-O(3)	75.88(13)	O(5)-B(2)-O(4)	111.9(5)
O(9)-Pb(1)-O(6)#2	76.31(15)	O(5)-B(2)-O(7)	107.1(4)
O(9)-Pb(1)-O(8)#3	98.47(13)	O(7)-B(3)-O(6)#2	120.1(5)
O(2)-Te(1)-O(4)	91.28(17)	O(8)-B(3)-O(6)#2	119.3(5)
O(9)-Te(1)-O(2)	99.46(18)	O(8)-B(3)-O(7)	120.6(5)
O(9)-Te(1)-O(4)	97.34(18)	O(1)#7-B(4)-O(6)	118.3(5)

O(2)-B(1)-O(1)	107.7(5)	O(5)-B(4)-O(1)#4	128.2(5)
O(3)-B(1)-O(1)	106.1(5)	O(5)-B(4)-O(6)	113.4(5)
O(3)-B(1)-O(2)	113.6(5)		

Symmetry transformations used to generate equivalent atoms:

#1 1-X,1-Y,-Z #2 1+X,+Y,+Z #3 +X,1+Y,+Z #4 1-X,-Y,1-Z

#5 1-X,1-Y,1-Z #6 -1+X,1+Y,+Z #7 +X,-1+Y,+Z

Table S4. Assignment of the absorption peaks observed in the IR spectrum of $PbTeB_4O_9$:

Mode description	Absorption peaks (cm^{-1}) for $PbTeB_4O_9$
$v_{as}(BO_3)$	1453, 1362
$v_{as}(BO_4)$	1244, 1081
$v_s(BO_3)$	950
$v_s(BO_4)$	850
$\delta_{out}(BO_3)$	614
$\delta(BO_4, BO_3)$	582, 546
$V_{s,\,as}(TeO_3)$	682, 460

Table S5. Inorganic Tellurium borates summarized according to the ICSD with the version of 5.0.0 (the latest release of ICSD-2022/08).[13]

Compound	Space group	B−O group	Te−O group	Te−B−O group	Birefringence
Tellurate Borates					
$Na_2Y_2TeB_2O_{10}$	$P2_1/c$	$[BO_3]$	$[TeO_6]$	0D $[TeO_4(BO_3)_2]$ groups	0.040
$Na_2Dy_2TeB_2O_{10}$	$P2_1/c$	$[BO_3]$	$[TeO_6]$	0D $[TeO_4(BO_3)_2]$ groups	n/a
$Na_2Ho_2TeB_2O_{10}$	$P2_1/c$	$[BO_3]$	$[TeO_6]$	0D $[TeO_4(BO_3)_2]$ groups	n/a
$Na_2Er_2TeB_2O_{10}$	$P2_1/c$	$[BO_3]$	$[TeO_6]$	0D $[TeO_4(BO_3)_2]$ groups	n/a
$Na_2Tm_2TeB_2O_{10}$	$P2_1/c$	$[BO_3]$	$[TeO_6]$	0D $[TeO_4(BO_3)_2]$ groups	n/a
$Na_2Yb_2TeB_2O_{10}$	$P2_1/c$	$[BO_3]$	$[TeO_6]$	0D $[TeO_4(BO_3)_2]$ groups	n/a
$Na_2Lu_2TeB_2O_{10}$	$P2_1/c$	$[BO_3]$	$[TeO_6]$	0D $[TeO_4(BO_3)_2]$ groups	n/a
$Pb_2Mg_2TeB_2O_{10}$	*Cmca*	$[BO_3]$	$[TeO_6]$	0D $[TeO_4(BO_3)_2]$ groups	0.077

$Ba_2Mg_2TeB_2O_{10}$	*Cmca*	$[BO_3]$	$[TeO_6]$	0D $[TeO_4(BO_3)_2]$ groups	0.046
$Sr_5TeO_2(BO_3)_4$	*P*4/*mnc*	$[BO_3]$	$[TeO_6]$	0D $[TeO_2(BO_3)_4]$ groups	0.048
Bi_3TeBO_9	$P6_3$	$[BO_3]$	$[TeO_6]$	No connection	0.056
$Ca_{13}Te_{4.42}O_{15}(BO_3)_4(OH)_3$	$P6_3/m$	$[BO_3]$	$[TeO_6]$, $[TeO_3]$ and $[TeO_3(OH)]$	No connection	n/a
$Ba_4B_8TeO_{19}$	*Cc*	$[B_4O_{11}]$	$[TeO_6]$	3D frameworks	0.055
Tellurite Borates					
$LaTeBO_5$	*Pbca*	$[BO_3]$	$[TeO_4]$	0D $[Te_2O_4(BO_3)_2]$ groups	0.080
TeB_4O_8	*C*2/*c*	$[BO_4]$	$[TeO_4]$	3D frameworks	0.100[a]
$Rb_3BaTeB_7O_{15}$	$P2_1/n$	$[B_3O_8]$	$[TeO_3]$	2D $[TeB_7O_{15}]$ layers	0.035
$PbTeB_4O_9$	$P\bar{1}$	$[B_4O_{10}]$	$[TeO_3]$	2D $[TeB_4O_9]$ layers	0.099

[a]These data were calculated by using the first-principles calculations under the same calculation parameters with $PbTeB_4O_9$.

Table S6. Contribution percent w (%) of different units in $PbTeB_4O_9$ calculated by the real-space atom-cutting method.

unit	[Pb−O]	[Te−O]	[B−O]
w (%)	7%	56%	37%

Figure S1. The arrangement of [PbO_9] polyhedra (a, b) and [TeO_3] polyhedra (c, d) in the structure.

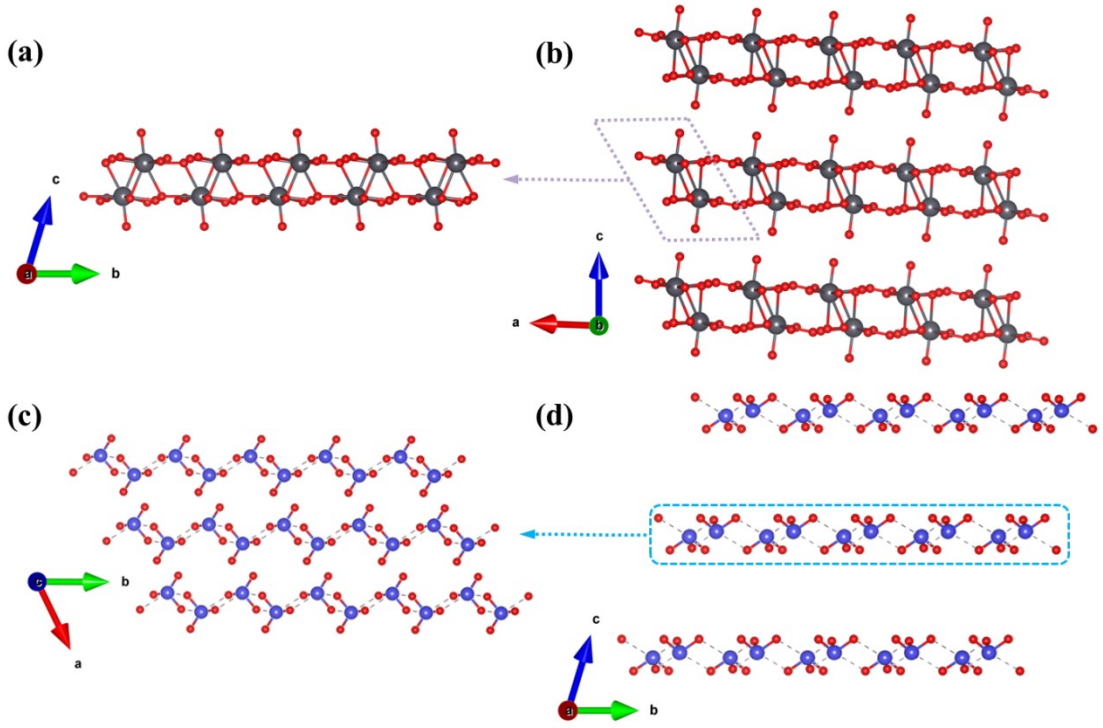

Figure S2. The types of [B_4O_{10}] FBBs from different borates.[14]

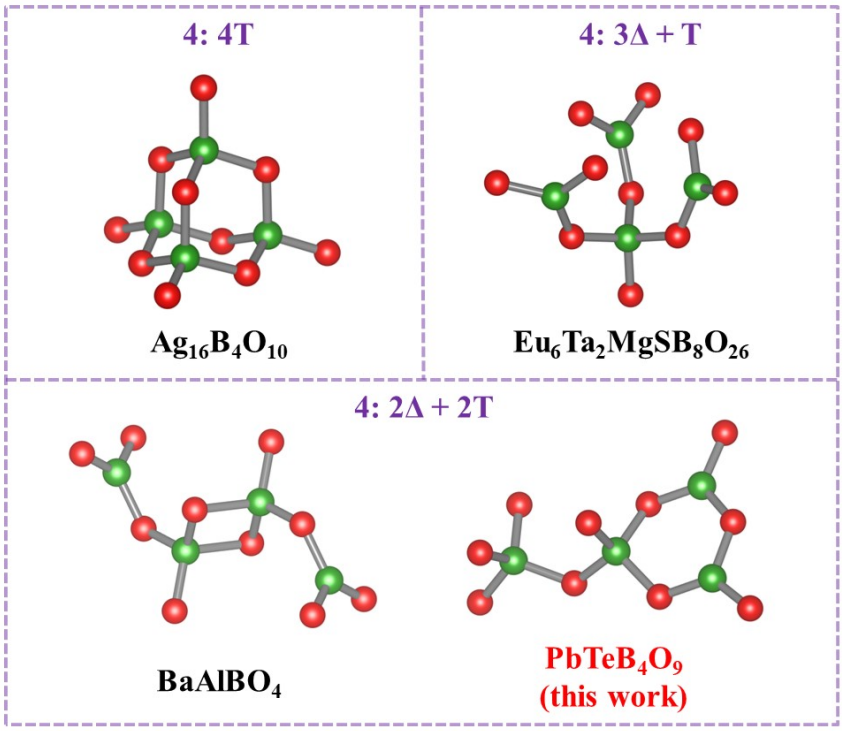

Figure S3. (a) 2D $[B_4O_8]_\infty$ layer with 18-MR consisting of $[B_4O_{10}]$ FBBs in $PbTeB_4O_9$; (b) 2D $[B_4O_6F]_\infty$ layer with 18-MR consisting of $[B_4O_8F]$ FBBs in NaB_4O_6F. (Blue tetrahedra are $[BO_4]$ units and $[BO_3F]$ units; green triangles are $[BO_3]$ units.)

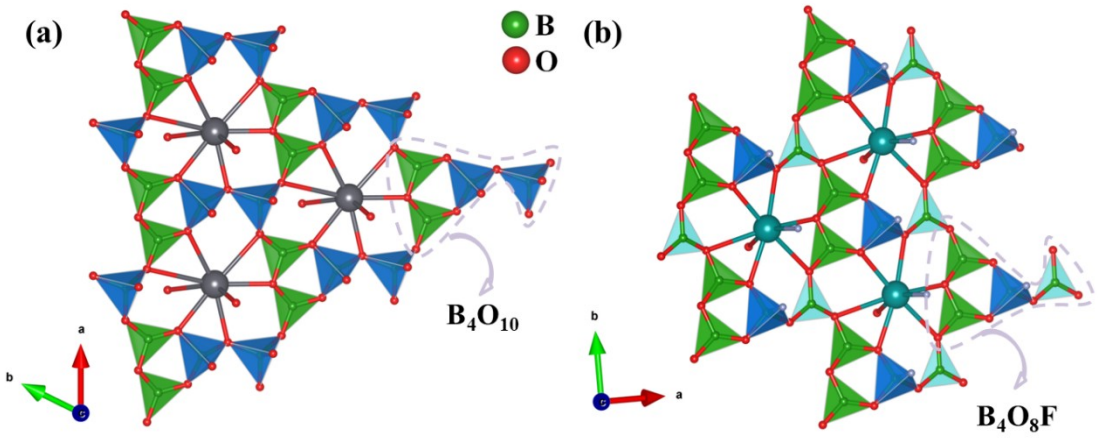

Figure S4. Powder XRD patterns of experimental and calculated results for $PbTeB_4O_9$.

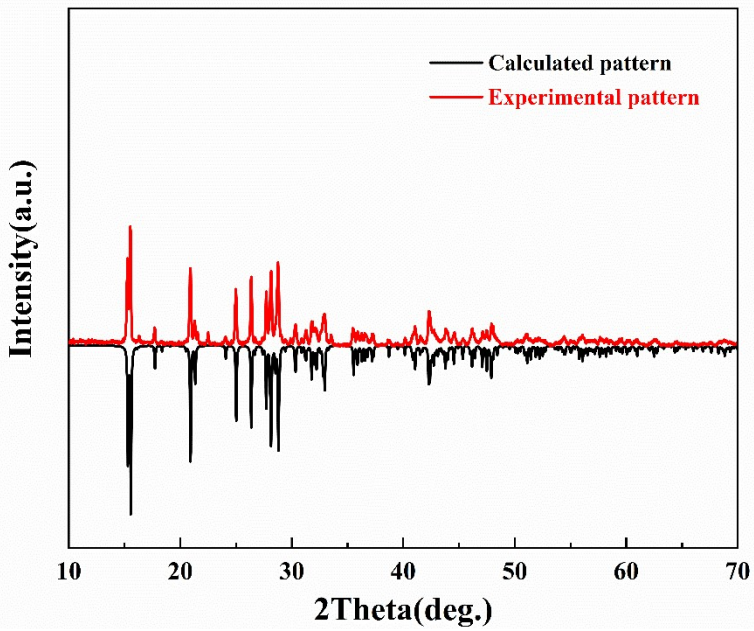

Figure S5. (a) TG-DSC curves of $PbTeB_4O_9$; (b) XRD patterns annealed at 520 and 580 °C for 24 h, respectively (comparing with calculated pattern).

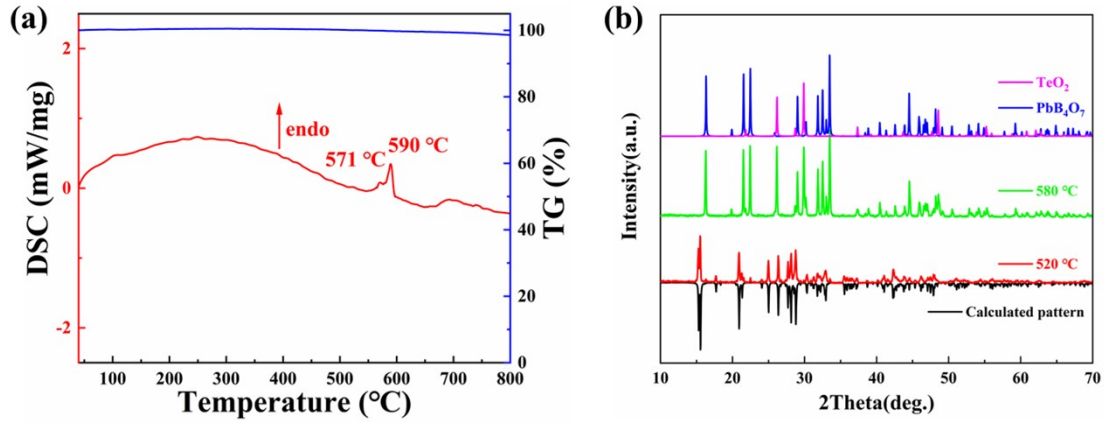

Figure S6. IR spectrum of $PbTeB_4O_9$. For $PbTeB_4O_9$, the peaks at 1453 and 1362 cm^{-1} can be assigned to the asymmetric stretching of the $[BO_3]$ groups. The peaks at 1244 and 1081 cm^{-1} can be attributed to the asymmetric stretching of the $[BO_4]$ units. The peaks at 950 and 850 cm^{-1} can be attributed to the symmetric stretching of B−O in the $[BO_3]$ and $[BO_4]$ units, respectively. The bands associated with the $[BO_3]$ and $[BO_4]$ out-of-plane and in-plane bending modes are located at about 546–614 cm^{-1}. The peak observed at 682 cm^{-1} is assigned to the doubly degenerate anti-symmetric stretching vibration mode of the $[TeO_3]$ units, while the peak at 460 cm^{-1} is attributed to the symmetric stretching vibration mode of the $[TeO_3]$ units. All these results are in good agreement with those reported before.[13i,k,15]

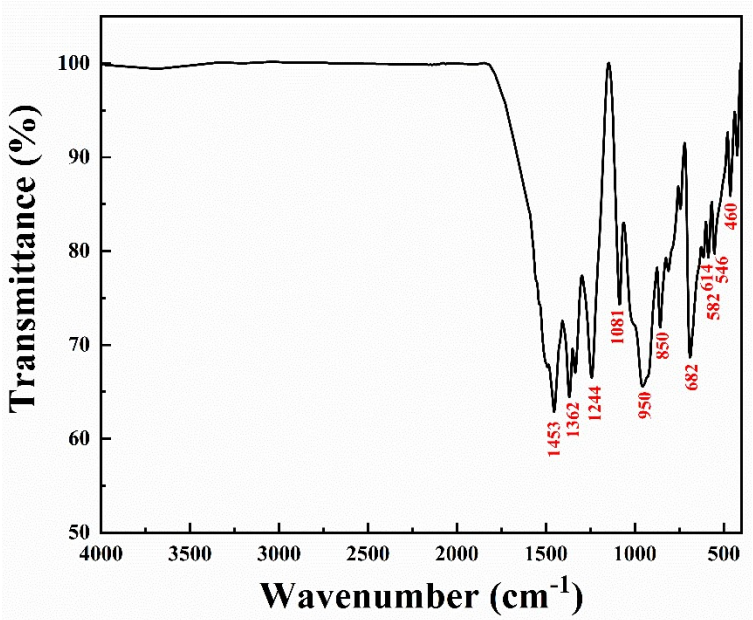

Figure S7. Energy dispersive X-ray spectroscopy of $PbTeB_4O_9$.

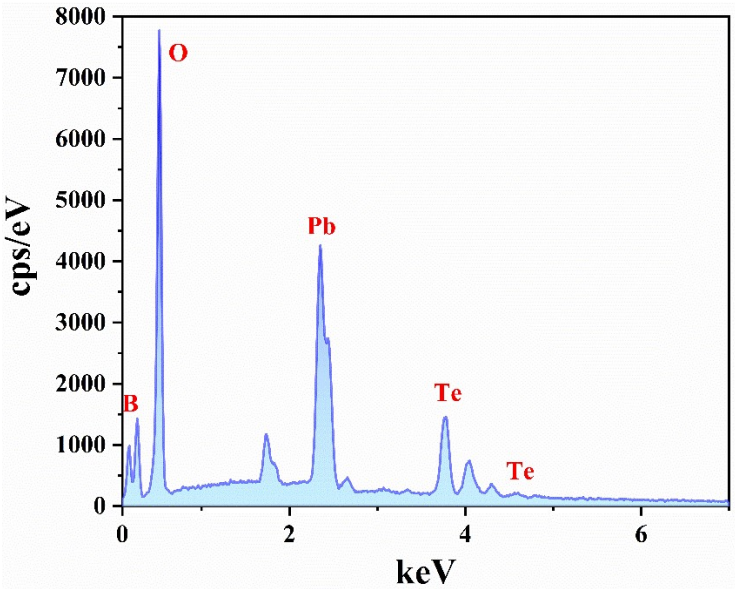

Figure S8. UV-vis-NIR diffuse reflectance spectrum of $PbTeB_4O_9$.

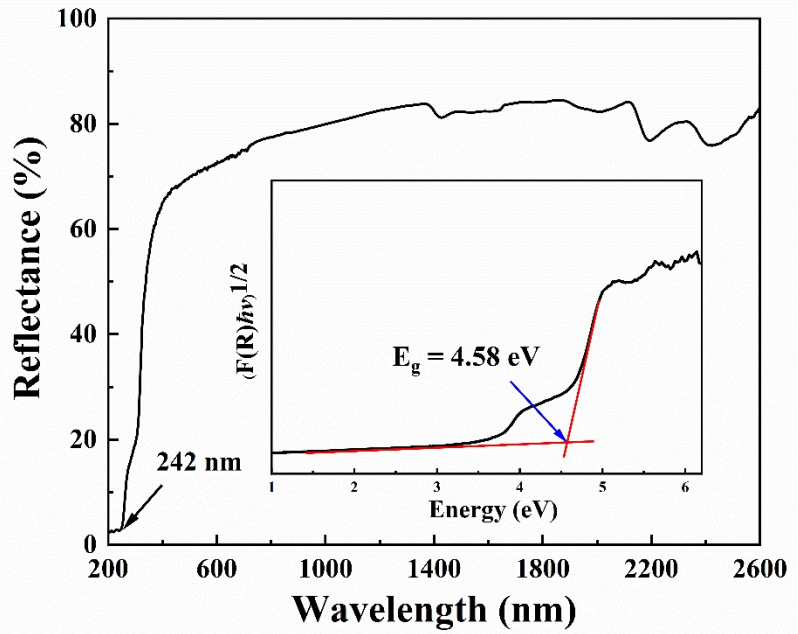

Figure S9. (a) Calculated band structure of $PbTeB_4O_9$. (b) Partial density of states (PDOS) of $PbTeB_4O_9$.

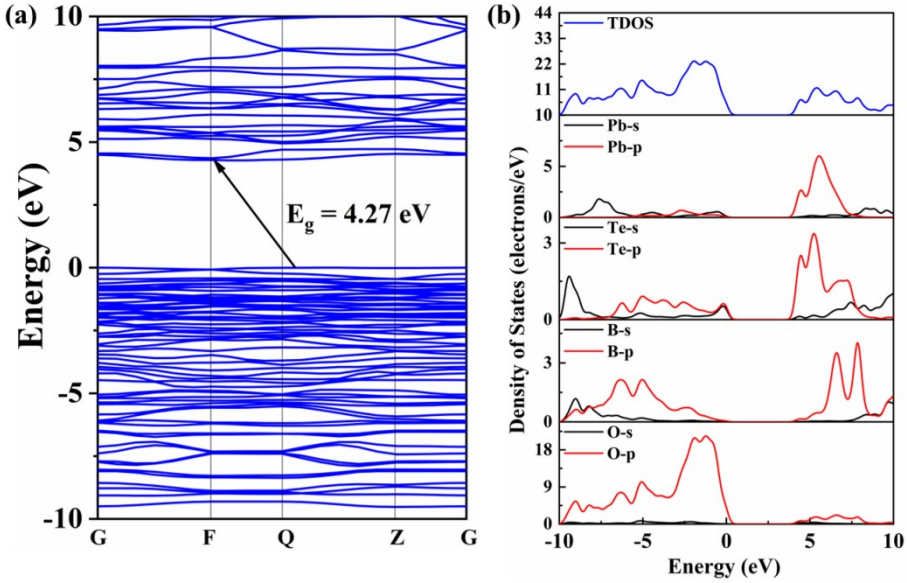

Figure S10. Electron localization function diagram of Pb atoms.

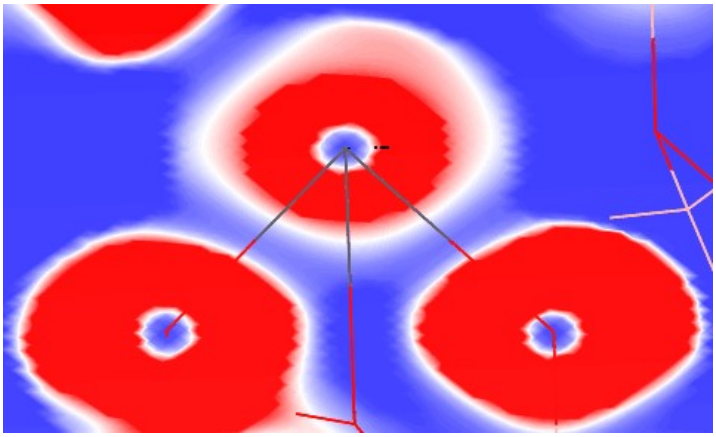

1 SAINT, *version 7.60A*, Bruker Analytical X-ray Instruments, Inc., Madison, WI, 2008.

2 O. V. Dolomanov, L. J. Bourhis, R. J. Gildea, J. A. K. Howard and H. Puschmann, *J. Appl. Crystallogr.* 2009, **42**, 339−341.

3 A. L. Spek, *J. Appl. Crystallogr.*, 2003, **36**, 7−13.

4 N. E. Brese, M. O. Keeffe, *Acta Crystallogr. B*, 1991, **47**, 192−197.

5 S. J. Clark, M. D. Segall, C. J. Pickard, P. J. Hasnip, M. J. Probert, K. Refson and M. C. Payne, *Z. Kristallogr.*, 2005, **220**, 567−570.

6 B. G. Pfrommer, M. Côté, S. G. Louie and M. L. Cohen, *J. Comput. Phys.*, 1997, **131**, 233−240.

7 J. P. Perdew, K. Burke and M. Ernzerhof, *Phys. Rev. Lett.*, 1996, **77**, 3865.

8 J. S. Lin, A. Qteish, M. C. Payne and V. Heine, *Phys. Rev. B*, 1993, **47**, 4174.

9 A. M. Rappe, K. M. Rabe, E. Kaxiras and J. D. Joannopoulos, *Phys. Rev. B*, 1990, **41**, 1227.

10 H. J. Monkhorst, J. D. Pack, *Phys. Rev. B*, 1976, **13**, 5188.

11 E. D. Palik, *Handbook of Optical Constants of Solids*; Academic Press: New York, 1985.

12 J. Lin, M-H. Lee, Z-P. Liu, C. T. Chen and C. J. Pickard, *Phys. Rev. B*, 1999, **60**, 13380−13389.

13 (a) J. H. Feng, C. L. Hu, X. Xu, F. Kong and J. G. Mao, *Inorg. Chem.*, 2015, **54**, 2447−2454; (b) M. Wen, H. P. Wu, C. Hu, Z. H. Yang and S. L. Pan, *Inorg. Chem.*, 2019, **58**, 11127−11132; (c) R. L. Tang, C. L. Hu, J. H. Feng, Z. Fang, Y. Chen, F. Kong and J. G. Mao, *Dalton Trans.*, 2020, **49**, 3743−3749; (d) M. J. Xia, X. X. Jiang, Z. S. Lin and R. K. Li, *J. Am. Chem. Soc.*, 2016, **138**, 14190−14193; (e) W. M. Dong, Y. J. Sun, B. Wang, M. Q. Zhu, J. Li, X. G. Xu and J. Y. Wang, *Inorg. Chem.*, 2022, **61**, 8870−8878; (f) M. Daub, M. Krummer, A. Hoffmann, L. Bayarjargal and H. Hillebrecht, *Chem. - Eur. J.*, 2017, **23**, 1331−1337; (g) M. Weil, G. Heymann and H. Huppertz, *Chem. - Eur. J.*, 2016, **22**, 3574−3579; (h) L. L. Liu, J. Young, M. Smeu and P. S. Halasyamani, *Inorg. Chem.*, 2018, **57**, 4771−4776; (i) J. K. Wang, H. P. Wu, H. W. Yu, Z. H. Hu, J. Y. Wang and Y. C.

Wu, *Dalton Trans.*, 2021, **50**, 12404−12407; (j) R. Ziegler, G. Heymann, H. Huppertz, *Z. Anorg. Allg. Chem.*, 2022, **648**, e202200229; (k) J. Sun, M. Mutailipu, S. C. Cheng, Z. H. Yang and S. L. Pan, *Dalton Trans.*, 2020, **49**, 8911−8917.

14 (a) A. Kovalevskiy, C. L. Yin, J. Nuss, U. Wedig and M. Jansen, *Chem. Sci.*, 2020, **11**, 962−969; (b) Z.-H. Shi, Y. Chi, M. Yang, W. L. Liu and S.-P. Guo, *Inorg. Chem.*, 2020, **59**, 3532−3536; (c) F. J. Guo, J. Han, S. C. Cheng, S. J. Yu, Z. H. Yang and S. L. Pan, *Inorg. Chem.*, 2019, **58**, 8237−8244.

15 (a) S. Cho, S. Park, Y. Kuk and K. M. Ok, *Mater. Today Phys.*, 2023, **34**, 101075; (b) B. Zhang, J. H. Wu, C. L. Hu, Y. F. Li, F. Kong and J. G. Mao, *Inorg. Chem. Front.*, 2023, **10**, 1328-1337; (c) C. A. Chen, W. F. Liu and G. Y. Yang, *Chem. Commun.*, 2022, **58**, 8718-8721; (d) C. Wu, X. X. Jiang, L. Lin, W. Y. Dan, Z. S. Lin, Z. P. Huang, M. G. Humphrey and C. Zhang, *Angew. Chem. Int. Ed.*, 2021, **60**, 27151-27157; (e) J. F. Zhou, P. F. Gong, M. J. Xia, A. M. Ji, L. F. Zhang, H. Q. Wu and Q. Wu, *Inorg. Chem.*, 2023, **62**, 8931−8939.